Journal of Materials Chemistry B

Accepted Manuscript

This article can be cited before page numbers have been issued, to do this please use: L. Naszályi Nagy, A. Polyák, J. Mihály, Á. Szécsényi, I. C. Szigyártó, Z. Czégény, E. Jakab, P. Németh, B. Magda, P. T. Szabó, Z. Veres, K. Jemnitz, I. Bertóti, R. P. Jóba, G. Trencsényi, L. Balogh and A. Bóta, *J. Mater. Chem. B*, 2016, DOI: 10.1039/C6TB01102K.

ROYAL SOCIETY OF CHEMISTRY

www.rsc.org/materialsB

View Article Online
DOI: 10.1039/C6TB01102K

View Article Online
DOI: 10.1039/C6TB01102K

Journal Name

ARTICLE

Silica@zirconia@poly(malic acid) nanoparticle: a promising nanocarrier for theranostic applications

Received 00th January 20xx,
Accepted 00th January 20xx

DOI: 10.1039/x0xx00000x

www.rsc.org/

L. Naszályi Nagy,[a,†] A. Polyak,[b,c] J. Mihály,[a] Á. Szécsényi,[a,‡], I. Cs. Szigyártó,[a] Zs. Czégény,[a] E. Jakab,[a] P. Németh,[a] B. Magda,[d] P. Szabó,[d] Zs. Veres,[e] K. Jemnitz,[e] I. Bertóti,[a] R. P. Jóba,[f] Gy. Trencsényi,[g] L. Balogh,[b] and A. Bóta[a]

Silica@zirconia@poly(malic acid) nanocarriers of 130 nm mean diameter were designed, synthesized and characterized for the targeted delivery of diagnostic and therapeutic ^{99m}Tc isotope to folate-overexpressing tumors. An important achievement was that a multifunctional L-(–)-malic-acid-based copolymer was formed *in situ* at the surface of the inorganic cores in a single synthetic step incorporating L-(-)-malic acid, β-cyclodextrin rings, folic acid moieties, and polyethylene glycol chains. Morphological and in-depth structural analysis of the particles proved their core@shell structure. Stability experiments in aqueous media evidenced that stable suspensions can be obtained from the lyophilized powder in 10 mM phosphate buffer at pH 7.4. During 14-day degradation experiments, the nanoparticles were found to be slowly dissolving (including inorganic core) in saline and also in total cell medium. *In vitro* toxicity assay on hepatocytes showed a concentration-dependent decrease of cell viability down to 63±1% at the highest applied concentration (0.5 mg/ml). Proof of concept experiments of technetium-99m radiolabelling and *in vivo* labelling stability are presented.

Introduction

Application of nanotechnology in the field of theranostics has become a promising strategy for personalized medicine[1–4]. Various multifunctional nanoparticles are synthesized for targeted drug delivery[5,6]. However those, which combine diagnostic and therapeutic functionalities (nanotheranostics) and can be used for advanced *in vivo* imaging techniques (e.g. single photon emission computed tomography coupled to computer tomography, SPECT/CT)[7,8] are the most important. The biodistribution of nanotheranostics is quantitatively evaluated on the basis of radiation detection, which enables excellent evaluation and planning of dosage when the same nanocarrier is used for drug delivery.

Nanocarriers used in theranostic applications are of various compositions: inorganic[9,10], organic[11–13], biological[14] as well as their combinations[15,16]. The main advantages of inorganic nanoparticles are their well-defined size and shape, longer shelf-life and the conservation of their integrity in biological medium. On the other hand the degradability has become a priority to avoid the accumulation of these materials in the body causing unknown long-term effects. Biodegradability is an inherent advantage of most organic and biological nanocarriers.

Silica is, however, one of the exceptional biodegradable inorganic materials[17,18], which has several additional advantages, too: it is biocompatible, its surface modification is relatively easy[19,20], and further, the diameter and shape of nanoparticles can be easily controlled (18-1000 nm)[21,22].

Zirconia, though not biodegradable, is another ceramic material used in medical applications as implant[23–25]. Few papers mention its use as a drug delivery nanocarrier[26]. In fact, pure ZrO_2 colloid with uniform size and shape could only be obtained with a particle diameter above 200 nm[27,28]. However, when silica is used as a template, continuous zirconia shell may be deposited on its surface and particles can be obtained with well-controlled size[29,30].

We aimed at the preparation of a new complex nanocarrier for the targeted delivery of theranostic ^{99m}Tc isotope to folate overexpressing tumours by combining the advantageous properties of silica, zirconia with those of degradable polymers. Our concept was to cover Stöber silica core of nearly 100 nm diameter with zirconia (silica@zirconia), and then form

[a] *Institute of Materials and Environmental Chemistry, Research Centre for Natural Sciences, Hungarian Academy of Sciences, Budapest, H-1117 Magyar Tudósok Blvd 2, Hungary. E-mail: nagy.naszalyi.livia@ttk.mta.hu; Tel: +36-1-382-6836*
[b] *Department of Radiobiology, National Research Institute for Radiobiology and Radiohygiene, Budapest, H-1221 Anna Str 5, Hungary.*
[c] *Department of Nuclear Medicine, Hannover Medical School, Hannover, Carl-Neuberg-Str 1, D-30625, Germany*
[d] *Institute of Organic Chemistry, Research Centre for Natural Sciences, Hungarian Academy of Sciences, Budapest, H-1117 Magyar Tudósok Blvd 2, Hungary.*
[e] *Department of Nuclear Medicine, Semmelweis University, Budapest, H-1082 Üllői Rd 78, Hungary.*
[f] *Department of Nuclear Medicine, University of Debrecen, Debrecen, H-4032 Nagyerdei Blvd 98, Hungary.*
† Present address: MTA-SE Molecular Biophysics Research Group, Budapest, Tűzoltó Str 37-47, H-1094, Hungary. E-mail: lnaszalyi@gmail.com
‡ Present address: Department of Chemical Engineering, Delft University of Technology, Delft 2600 AA, The Netherlands.
Electronic Supplementary Information (ESI) available: details of characterization procedures; DLS size distribution functions, FTIR, TG/DTA, XPS spectra, TEM pictures and biodistribution data. See DOI: 10.1039/x0xx00000x

View Article Online
DOI: 10.1039/C6TB01102K

a new poly(ester-amide) outer shell to be able to chelate ^{99m}Tc ions and achieve multiple functionalities (Scheme 1).

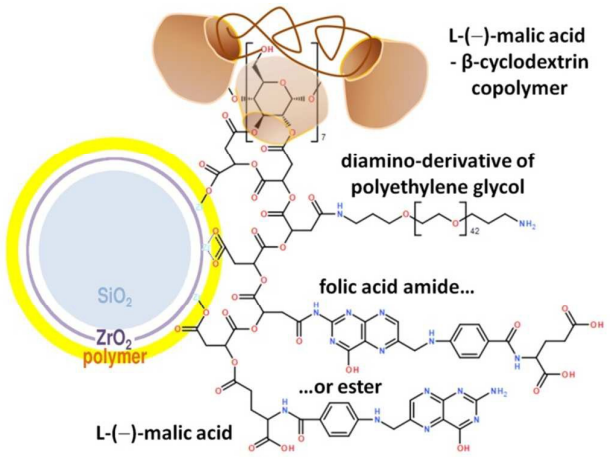

Scheme 1 Schematic representation of the silica@zirconia@polymer complex nanocarrier. The malic acid-based poly(ester-amide) copolymer is formed in a one-step surface catalysed condensation of the components.

We chose the components of the polymeric shell on the basis of our previous (non-published) experience. L-(–)-malic acid is a potentially interesting, biocompatible material, from which a low molecular weight homopolymer can be easily formed by polycondensation[31]. According to our observations malic acid adsorbs strongly at the zirconia surface and still participates in homopolymerization reaction allowing the formation of surface polymeric shell. Unfortunately, the homopolymer of malic acid (in bulk or at the surface of ZrO_2) undergoes rapid hydrolysis in water due to the autocatalytic effect of multiple unreacted carboxyl groups. This is why it cannot be used as a drug delivery polymer in itself. A polyol was chosen, therefore, to be the second component of the copolymer: β-cyclodextrin that should increase the conversion of polymerization (consumption of free carboxyl groups) and serve later as host for the complexation of small hydrophobic drug molecules[32]. Further components of the polymeric shell were: diamino derivative of polyethylene glycol (increases circulation time in blood stream[33]) and folic acid (achieves active targeting of folate receptor expressing tumours[34,35]). According to our hypothesis, these amine-containing components should further set back the degradation of the final copolymer thanks to the stability of amide bonds.

We report on the design, synthesis and physico-chemical characterization of the obtained complex nanocarriers (called thereafter CN) including stability and degradability conditions. Cell viability assay on hepatocyte cells and proof-of-concept SPECT/CT experiments are also presented.

Experimental section

Materials

Ethanol (a.r., 99.98%, max. 0.02% water, Reanal), ammonia solution (25%, a.r., Reanal), tetraethyl-orthosilicate (TEOS, puriss. GC, Sigma-Aldrich), zirconium-*n*-butoxide solution (TBOZ, 80 wt% in 1-butanol, Aldrich), L-(–)-malic acid (MA, puriss. >99.5%, Fluka Analytical), folic acid (FA, ≥97%, Sigma-Aldrich), N,N-dimethyl formamide (DMF, ACS-for analysis, min. 99.8%, Carlo Erba), β-cyclodextrin (β-CD, Cyclolab), dipropylamine-polyethylene glycol (diaminoPEG, SUNBRIGHT DE-034PA MW 2000, NOF Corporation), acetonitrile (HiPerSolv CHROMANORM for HPLC, VWR), $Na_2HPO_4{\times}2H_2O$ (Sigma), 1 N NaOH solution (for analysis, Carlo Erba), saline (SALSOL, 9 mg/ml NaCl, TEVA), penicillin-streptomycin mixture (cell culture tested, Sigma-Aldrich), methyl ethyl ketone (MEK, Reanal Ltd.), total cell medium (RPMI1640, Sigma-Aldrich), xylazine hydrochloride (CP-Pharma) and ketamine hydrochloride (CP-Pharma) were used as received. TEOS and TBOZ were kept under argon. Silica gel impregnated instant thin layer chromatography paper (ITLC-SG) was obtained from Pall Corporation. Millipore water (18.2 MΩcm, MilliQ System) was used during the experiments. Poly(L-(–)-malic acid – β-CD) copolymer (T40) was prepared and kindly provided by J. Telegdi[36]. The white solid has a melting point of 232.6°C and a specific rotation value of $[\alpha]_D^{25}$ = +41,5° (C=2, water) and a molar weight estimated on the basis of static light scattering measurement: 3530 Da. (The specific rotation of L-(–)-malic acid is $[\alpha]_D^{25}$ = -7.66° (C=2, acetone), melting point: 109.5°C.)

Preparation of complex nanocarriers

Silica sols with 112 nm mean particle diameter were prepared according to the procedure of Stöber *et al.*[21] using 10 ml of TEOS, 16 ml of ammonia solution and 250 ml ethanol.

Zirconia layer was deposited on the surface of silica particles with the adaptation of the procedure of Kim *et al.*[29]. 50 ml of silica sol (10.0±0.1 mg/ml) was diluted to 350 ml with ethanol under argon atmosphere in a stirred three-neck flask equipped with a dropping funnel. 1.5 ml of TBOZ was quickly diluted with 50 ml of ethanol in a mixing cylinder under argon in a glove box, and then was added dropwise into the vigorously stirred silica sol (1 h) at room temperature,

The reaction mixture was allowed to react for one hour. Then 360 mg of L-(–)-malic acid was added and the particles were separated by centrifugation at 5000 rpm for 5 min. The acid-capped inorganic particles were redispersed in 400 ml DMF solvent by ultrasonication for 2 min for further use.

Complex nanocarrier particles were prepared by dissolving 50 mg L-(–)-malic acid, 50 mg folic acid, 700 mg T40 copolymer and 50 mg diaminoPEG in 200 ml DMF solution of SiO_2@ZrO_2 (2.2±0.2 mg/ml particle concentration) (molar ratio of malic acid : folic acid : T40 copolymer : diaminoPEG = 1 : 0.3 : 0.53 : 0.067). The reaction mixture was heated up to 110°C, and stirred for one hour. After cooling down, the reaction mixture was purified by centrifugation and washed: once with DMF, three times with ethanol, and finally three times with water. The product was freeze-dried.

Characterization

Structure and stability of complex nanocarriers. Morphological investigation of nanocarriers was carried out on a MORGAGNI 268(D) (FEI, Eindhoven, Netherlands) transmission electron

View Article Online
DOI: 10.1039/C6TB01102K

microscope (TEM). Diluted samples were dropped and dried on carbon coated copper grids. The mean particle diameter and shell thickness analyses were performed using Olympus Soft Imaging Solution iTEM Software 5.0.

The stability of phosphate buffered CN suspensions against high electrolyte concentrations was checked by dynamic light scattering (DLS) measurements in an experimental design that was to imitate ^{99m}Tc labelling procedure. The isotope is eluted from the column in saline, thus phosphate buffer was chosen instead of PBS to avoid double saline content. DLS measurements were carried out on an AvidNano w130i instrument (30 mW diode laser emitting at 660 nm, avalanche photo diode detector placed at 90° (SABRe optics)). 0.5 mg/ml CN suspensions in 0-90 mM phosphate buffer were prepared and saline was added to each suspension in 0-1 volume ratio (resulting buffer concentrations indicated in Table S-1 in Electronic Supplementary Information, ESI).

The pH dependent zeta potential values of the samples were determined at 20 °C with a Malvern Zetasizer Nano ZS (Malvern, Worcs, UK) equipped with a He-Ne laser (λ = 633 nm) and a backscatter detector at fixed angle of 173°. 2.5 mg of CN was suspended in 20 ml Millipore water and ultrasonicated before the measurement. 20 ml of SiO_2, SiO_2@ZrO_2, and SiO_2@ZrO_2+MA samples in ethanol were centrifuged and the particles were suspended in Millipore water. HCl and NaOH solutions were used to adjust pH values between 3 and 10 (JENWAY 3540 Bench Combined Conductivity/pH Meter). Each symbol on the ζ-pH plot stands for the average and error of three measurements.

Characterization of the polymeric shell. The presence of functional groups was demonstrated with attenuated total reflectance Fourier-transform infrared (ATR-FTIR) spectroscopy using a BioRad FTS-60 spectrometer equipped with a DTGS (deuterated triglycine sulphate) detector and a single reflection diamond ATR accessory ('GladiATR' with 0.6×0.6 mm^2 active surface, PIKE Technologies, UK). Scans were performed in the wavenumber region 4000-350 cm^{-1}. In general, 4 cm^{-1} resolution and records of 128 scans were applied.

Thermogravimetry (TG) provided information about the polymerization conversion and the total mass of polymeric shell on the surface of nanoparticles. The CN powder was also thoroughly checked for traces of DMF solvent by coupled TG-MS measurements. TG measurements were performed on a modified Perkin-Elmer TGS-2 thermobalance and a HIDEN HAL 2/301 PIC quadrupole mass spectrometer. About 0.6 mg sample was placed into the platinum sample pan and heated at a 20°C min^{-1} up to 900°C in argon atmosphere. A small proportion of the evolved gas and vapor was introduced into the mass spectrometer through a glass lined metal capillary transfer line heated to 300°C. The quadrupole mass spectrometer operated at 70 eV electron energy.

Surface-specific elemental analysis information about the polymeric shell was deduced from X-ray photoelectron spectrum (XPS). X-ray photoelectron spectra were recorded on a Kratos XSAM 800 spectrometer operated at fixed analyser transmission mode using Mg $K_{\alpha1,2}$ (1253.6 eV) excitation. CN powder was fixed on a stainless steel sample holder by a vacuum-compatible double sided tape. Spectra were referenced to the energy of the C1s line of the hydrocarbon type carbon, present on the surface of the samples, set at 284.2 eV binding energy (see more details in ESI). Chemical states of the constituent elements were determined and assigned by using available references[37–39].

Dissolution of the polymeric shell. 6.7 mg CN sample was put on the top of centrifugal ultrafilter (Sartorius Stedim, VIVASPIN 500, 0.2 µm polyethersulfone, 5 µl dead-stop volume, prewashed with water) and 520 µl of either saline or total cell medium containing 5% penicillin-streptomycin was added to it. The filter was closed and left stirring at room temperature. On days 0-1-2-3-6-9-13 the samples were centrifuged at 12500 rpm for 30 min. Permeates were frozen till analyses, and the particles were resuspended in 500-500 µl saline or total cell medium. UV-visible spectroscopy, ATR-FTIR spectroscopy and high-performance liquid chromatography coupled to mass spectrometry (HPLC-MS/MS, see details in ESI) were performed on saline permeates. ATR-FTIR analysis was carried out on total cell medium samples. The surface of CN particles was analysed using ATR-FTIR spectroscopy at the end of degradation experiment. UV-visible spectra were recorded in a small-volume quartz cuvette on a Hewlett-Packard 8453 spectrophotometer.

Cell viability assay, radiolabelling and *in vivo* biodistribution. Toxicity of CN nanoparticles was tested with CytoTox Fluor™ Cytotoxicity Assay (Promega) on 96-well plates using MTT (3-(4,5-dimethylthiazol-2-yl)-2,5-diphenyltetrazolium bromide) dye and primary rat hepatocytes (see details in ESI).

For radiolabelling 0.5 mg of CN was suspended in 1 ml 10 mM Na_2HPO_4 phosphate buffer (pH 7.5). The sample was ultrasonicated for 10 min and its size distribution function was assessed by DLS measurement. 500 µl (680 MBq activity) of sterile generator-eluted pertechnetate ($^{99m}TcO^{4-}$) solution in saline was added to the nanocarrier suspension. The reduction was carried out with 37.5 µg $SnCl_2$ (×$2H_2O$) in 7.5 µl 0.05 M HCl. ^{99m}Tc-pertechnetate was derived from an UltraTechnekov (10.75 GBq) ^{99}Mo-^{99m}Tc generator (Covidien Imaging Solutions, USA). Labelling was performed within 20 minutes at room temperature. Radiochemical purity of the ^{99m}Tc-labelled nanocarrier was examined by means of thin-layer chromatography (TLC) (see details in ESI).

In vivo biodistribution of CN nanoparticles was investigated on three rats. Adult male Fischer-344 rats weighing 150–200 g were used for tumour-transplanted animal experiments. $5x10^6$ folate receptor overexpressing He/De tumour cells (rat epithelial liver carcinoma) in 150 µl saline were injected subcutaneously into the left thighs. The animals received humane care complying with the criteria outlined in the "Guidelines for the welfare and use of animals in cancer research"[40] (see further in ESI).

View Article Online
DOI: 10.1039/C6TB01102K

For SPECT/CT investigations, a 300 µl volume (122 MBq of activity/100 µg CN) of sterile radiolabelled CN suspension was administered into the tail vein of animals 1 hour post-labelling. Animals were anesthetized by administering a combination of xylazine and ketamine hydrochloride by the intraperitoneal route before the CN injection[8]. 30 minutes, 3 hours and 20 hours post injection whole-body fusion images were taken from the experimental animals using an AnyScan SPECT/CT hybrid scanner camera (Mediso Ltd., Hungary). Fused scans were processed using Interview Software (Mediso Ltd., Hungary). Region of interest (ROI) calculations were performed by outlining the borders of selected organs or tracts. Injected dose (ID)/whole organ values were estimated from the resulted ROI values.

Results and discussion

Structure and colloid stability of complex nanocarriers

The diameter of silica core was chosen to be around 100 nm to benefit from enhanced permeation and retention effect (EPR)[41]. The TEM picture of the CN powder shows nearly spherical particles with an average particle diameter of 112±10 nm (values obtained from TEM image analysis on 50 particles) (Fig.1). TEM pictures of SiO_2 and SiO_2@ZrO_2 particles are shown in Fig. S-1 in the ESI.

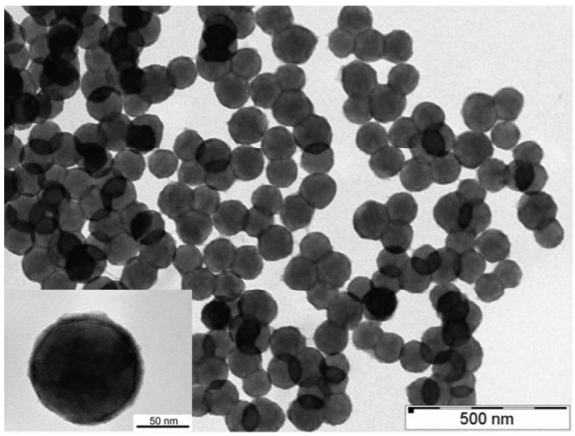

Figure 1 TEM pictures of complex nanocarriers.

According to these images, the polymeric shell covers the surface of the SiO_2@ZrO_2 spheres with an average thickness of 5.0±2.3 nm (measurement of thickness performed on the TEM image of 8 particles at 73 positions).

The deposition of surface layers was further confirmed by DLS measurements (see Fig. S-2a in ESI). The mean hydrodynamic diameter of silica particles in ethanol is 112 nm. This increases to 134 nm due to ZrO_2 deposition. The lyophilized CN particles redispersed in phosphate buffer show an increased mean hydrodynamic diameter of 275 nm and also a larger polydispersity index. This suggests that at least some of the particles underwent cross-linking during the polymerization step.

The changes in surface charge during synthetic procedure, as well, as the pH dependent surface charge conditions of the final product are well demonstrated by zeta potential vs. pH curves (Fig.2). The isoelectric point (IEP) of native silica particles is below pH 3 in agreement with previous results[42,43]. The IEP shifts to pH 7.5 after the deposition of zirconia. This corresponds to the value reported earlier for pure zirconia[44].

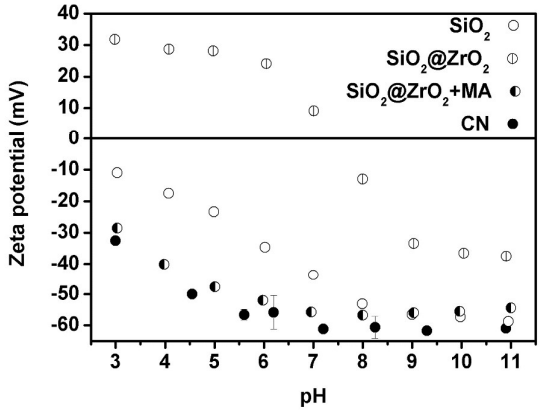

Figure 2 Zeta potential vs. pH analysis of the SiO_2 sol, the core@shell SiO_2@ZrO_2 sol before and after addition of malic acid (+MA), and the complex nanocarriers (CN). The experimental error is within the symbol's size except where marked.

After addition of malic acid to SiO_2@ZrO_2 the surface charge becomes lower than -30 mV in the whole pH range showing the high affinity of malic acid to zirconia surface. This is what has been assumed in advance as ZrO_2 is known to form strong surface interactions with citric acid, which is an analogue polydentate ligand[45]. The polymerization of multiple components resulted in a slight shift in the zeta potential-pH curve. This shows the maintained dominance of free carboxylic groups. The newly established chemical bonds and the overall surface structure of the particles was analysed by ATR-FTIR method (Fig.3).

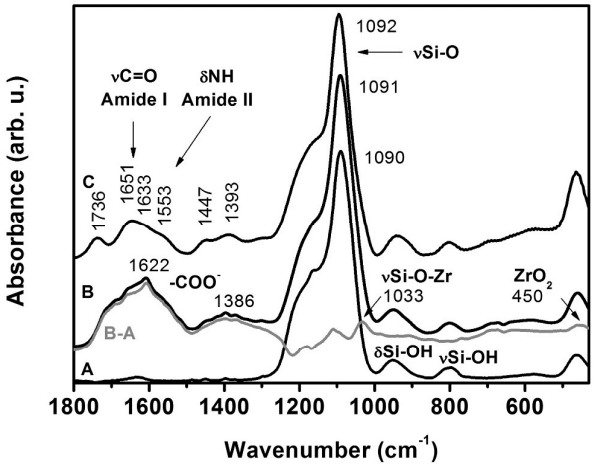

Figure 3 Fourier-transform infrared spectra of SiO_2 sol (A), SiO_2@ZrO_2 sol (B) and complex nanocarriers (CN) (C). The difference spectrum of SiO_2@ZrO_0–SiO_2 (B–A) is plotted in grey.

View Article Online
DOI: 10.1039/C6TB01102K

ATR-FTIR showed that the intensity of the vibrational bands characteristic to native silica surface (ν(Si-OH) absorption band at 950 cm^{-1} and ν(Si-O) at 798 cm^{-1}) is not reduced after zirconia deposition[29,46]. The detailed spectral analysis revealed a new band around 1033 cm^{-1}, related to (Si-O-Zr) asymmetric stretching. The broad band around 450 cm^{-1} corresponds to crystalline zirconia[47] (see subtracted spectrum, grey line in Fig.3). The surface structure of nanoparticles is significantly altered after polymerization: amide bonds appear at 1651 and 1553 cm^{-1}, and distinct carbonyl absorption is recorded at 1736 cm^{-1} (see spectrum C in Fig.3). These findings permit us to state that not only malic acid and T40 copolymer were integrated into the polymeric network through ester bonds, but amine-containing components have also been covalently linked in through amide bonds. The lack of signal at 73 m/z in TG-coupled mass spectrum confirmed the complete removal of DMF solvent from the CN powder.

Colloid stability. Preliminary stabilization experiments showed that despite the highly negatively charged particle surface in the pH range 3-11, CN particles could only be effectively suspended at neutral or basic pH. This apparent discrepancy can be understood if we consider the pK_a values of malic acid (pK_{a1} = 3.40, pK_{a2} = 5.20[48]). At the intrinsic pH of the CN particle suspension (3.2), surface carboxylic groups are mainly protonated which can lead to the formation of numerous intraparticular and interparticular H-bonds. This hypotheses is supported by the findings of Wohlfahrt who performed quantum chemical calculations for the modelling of H-bonding ability between carboxylic side chains in proteins, and stated that for repulsion between proteins pH>7 is necessary[49].
Size distribution functions obtained from DLS measurements evidenced that 10 mM phosphate buffer is appropriate for stabilizing the 0.5 mg/ml suspension of CN particles up to 77 mM NaCl concentration (see details in Figs.S-2b-d in ESI).

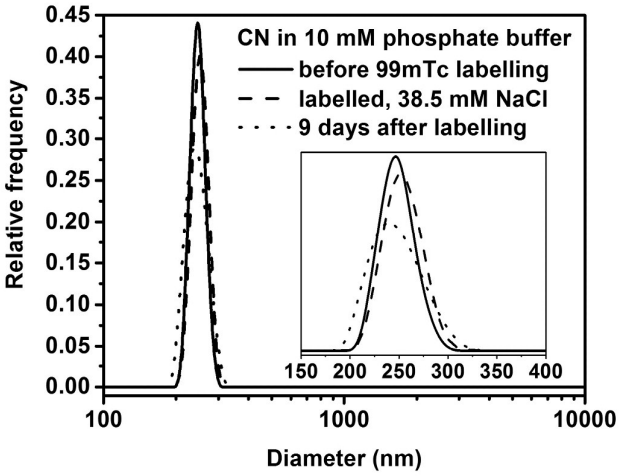

Figure 4 DLS size distribution functions of 0.5 mg/ml CN suspension in 10 mM phosphate buffer before (solid line; Z-ave: 275 nm PdI: 0.163) and after ^{99m}Tc labelling (38.5 mM saline) (dashed line; Z-ave: 274 nm. PdI: 0.111), and 9 days after labelling process kept at the ambient (dotted line; Z-ave: 269 nm PdI: 0.168).

The size distribution functions of the above suspension recorded repeatedly before and after radiolabeling with ^{99m}Tc show that the colloidal stability has been maintained for at least 9 days after labeling as intensity weighted Z-average particle size and polydispersity index do not change significantly (38.5 mM final NaCl concentration) (Fig.4).

Structure and composition of the polymeric shell

The elucidation of the copolymer structure required a more detailed study. We wished to prove the presence and the covalent binding of all the added components. Reference samples have been prepared for ATR-FTIR and TG measurements: the physical mixture of the polymeric shell components (M, identical molar ratio then for CN) and their bulk polymerization product (PM, same molar ratio than CN and P, heated to 110°C in DMF for 1 h, and then washed with ethanol). The parallel measurement of these enabled the identification of spectrum signals arising from the appearance of new bonds.
The superposition of absorbance bands of the monomers was observed in the ATR-FTIR spectrum of M. The bulk polymerization induced several important changes (Fig.S-3 in ESI). First, the dominating broad band around 1023 cm^{-1} belonging to O-C(H) stretching of the cyclodextrin indicates that an ester backbone has formed (this band was also a dominating band for T40 copolymer). Second, the loss of the separated -OH/-NH stretching bands at 3319-3542 cm^{-1}, and the appearance of characteristic amide bands at 1651 cm^{-1} ν(C=O) and 1575 cm^{-1} δ(-NH) suggest the formation of amide with the amino groups of folic acid and/or diaminoPEG. It is important to note, that when the polymerization occurs at the surface of zirconia shell (CN sample), the relative intensity of ester-amide- *vs*. carboxylate-bands are reversed. This indicates that zirconia plays a definite role in the polymerization reaction, probably by forming metal-carboxylate complexes on its surface[50].
Similar information could be obtained from the thermal decomposition experiments of M, PM and CN samples (Fig.S-4 in ESI). New degradation peaks appear for PM (e.g. intensive peak at 340°C), than observed previously for the mixture of monomers[51-53] or for malic acid homopolymer[54]. For CN particles the degradation peaks are further shifted towards higher temperatures indicating higher polymerization conversion. Thus, thermogravimetric results support that the presence of zirconia surface interferes notably in polymerization process. The use of zirconia as a catalyst in liquid phase esterification of fatty acids was reported by Takahashi and coworkers[55]. However, our observation is that the zirconia surface itself becomes covered by a covalently bound polymer that cannot be completely removed of it anymore (the zeta potential of the particles remains highly negative in the pH range 3-11 after multiple dialyses).
The surface elemental composition of the CN sample was analysed using X-ray photoelectron spectroscopy (see raw spectra in Fig.S-5 in ESI). This surface sensitive technique mainly provides information about the top 10 nm of the

View Article Online
DOI: 10.1039/C6TB01102K

sample (more than half of the information coming from the first nm), and could hardly detect the presence of the SiO_2@ZrO_2 core (Table 1). This result supports our observation based on TEM pictures that the coverage of the particles with polymer is complete. However, there are differences between the experimental (derived from XPS data) and theoretical composition of the polymeric shell (theoretical: 53.2% C, 45.4% O and 1.4% N).

Table 1 Composition of the polymeric shell evaluated from XPS measurement

Peak	Position BE (eV)	FWHM (eV)	Raw Area (CPS)	RSF	x_{exp} %	$x_{p.\,exp}$ %
C 1s C-CH	284.1	2.10	2672	0.318	16.6	
C 1s C-O	285.8	2.10	3438	0.318	21.3	65.7**
C 1s C=O	287.7	1.94	1517	0.318	9.4	
C 1s C-OO	288.9	1.94	680	0.318	4.2	
O 1s O-C; HO-C	531.7	2.06	9364	0.936	19.7	34.4**
O 1s O=C	533.0	1.97	3483	0.936	7.3	
O 1s O-Zr	530.0	2.10	4966	0.936	10.5	-
O 1s O-Si	532.1	1.96	1527	0.936	3.2	-
Zr 3d (5/2)	182.1	2.15	*8681	2.796	6.1	-
Si 2p Si-O	103.6	2.10	208	0.371	1.1	-
Si 2p Si-O-Et	100.3	2.10	104	0.371	0.6	-

*sum (5/2+3/2); **calculated by substraction of Si-O-Et , SiO_2 and ZrO_2 contributions;
BE: binding energy. FWHM: Full-width half-maximum. RFS: relative sensitivity factor.
x: atomic percent. exp: experimental value. p: polymeric shell.
th: theorethical value (here only carbon and oxygen)

The presence of nitrogen could not be evidenced by our XPS measurement (the detection limit is nearly 1 at% N). We have considered the possibility of segregation inside the polymeric shell, and calculated the atomic composition of monomers (Table S-2 in ESI). The experimental results agree best the atomic composition of diaminoPEG, which might be in excess on the particle surface. Similar effect has been described previously for poly(lactic-co-glycolic acid) surfaces prepared by spin coating from a homogeneous solution of polyester and PEG chains[56].

The presence of PEG chains at the surface of CN particles may ensure long circulation time in blood stream, which is favourable for theranostic application. On the other hand, these results indicate that folic acid may not be available at the particle surface in sufficiently high amount for folate receptor targeting. Further biological studies will be dedicated to the investigation of this issue.

Dissolution of the polymeric shell

According to our preliminary experiments the homopolymer of L-(–)-malic acid decomposes completely during 20 min of ultrasonication in water, even when formed by surface catalysis on silica@zirconia nanoparticles. (However, a monolayer of malic acid remains adsorbed at the particle surface.) The same occurs when a copolymer is formed at the surface of the particles using L-(–)-malic acid and β-cyclodextrin monomers with the addition of diamino-PEG and folic acid for the last 10 min of the polymerization step (Fig.S-6 in ESI). The rapid dissolution is a disadvantage for a pharmaceutical carrier candidate. We overcame this problem by using pre-formed copolymer of L-(–)-malic acid and β-cyclodextrin, and with the presence of amine-bearing components throughout all the polymerization process. These nanocarriers did not lose their polymer coverage during 20 min of ultrasonication in water according to TEM investigation. We examined thereafter their dissolution in saline and total cell medium during a two-week period.

The dissolution rate of the polymeric shell in saline was analysed with mass spectrometry (Fig.5).

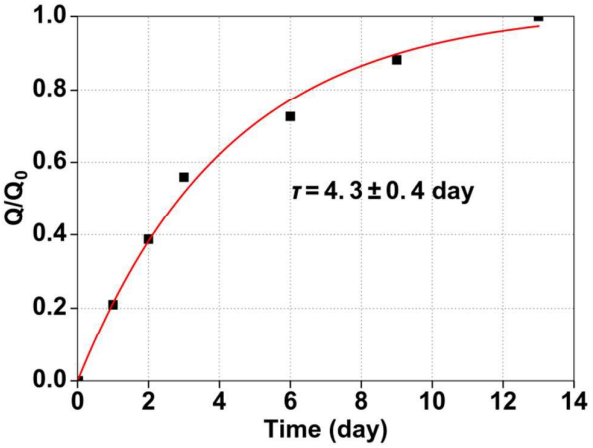

Figure 5 Fraction of released malic acid in saline (symbols) and fitted curve (line). The fraction of dissolved malic acid was calculated taking the last measurement point at 10000 min for 100%.

The experimental points were fitted with the following equation:

$$Q/Q_0 = A[1 - e^{-kt}]$$

where Q and Q_0 are the quantity of released malic acid till a given time point and till the 14th day of experiment, respectively, A is a constant, k is the dissolution rate, whose reciprocal is τ, the time constant. Malic acid release can be described with a time constant of 4.3 ± 0.4 day at 25°C under the given parameters (k = 0.232 ± 0.02 day^{-1}, $\tau_{1/2}$ = 2.98 ± 0.3 day). Thus, half of the polymeric shell dissolves within three days, if the particles are daily put into fresh saline.

Permeates in saline were further analysed by UV-visible spectroscopy (Fig.6a). The absorption curves show three main peaks at 210-219 nm, 239 nm and between 271-298 nm. The absorption band of malic acid (and that of T40) is near 210 nm (Fig.6b). It appears as a shoulder of the peak at 219 nm in the spectra of permeates. Folic acid absorbs light at 219 nm and at 276 nm (depending slightly on pH[57]). β-CD has a weak absorption band near 240 nm, but it has two more absorption regions under 210 nm and between 300-320 nm. The relative intensity of these peaks in permeate spectra is varying in time confirming compositional changes during the dissolution. It is to note, that the most intensive absorption peak in all permeates observed at 239 nm cannot be assigned to any of the polymeric shell components. We thereafter examined the absorption bands of amide bonds and C=C double bonds, but they proved to be at lower wavelength. Finally, we prepared a mixture of an aqueous suspension of crystalline ZrO_2 powder (obtained by the method of Zhou *et al.*[58]) with malic acid

View Article Online
DOI: 10.1039/C6TB01102K

solution and a second mixture with folic acid solution (Fig.6b). We observed the appearance of a new absorption band in the ZrO_2+FA mixture at 239 nm, but not in ZrO_2+MA. In fact, folic acid is known to form metal ion complexes[57,59], but this is the first proof of the formation of zirconium-folate complex.

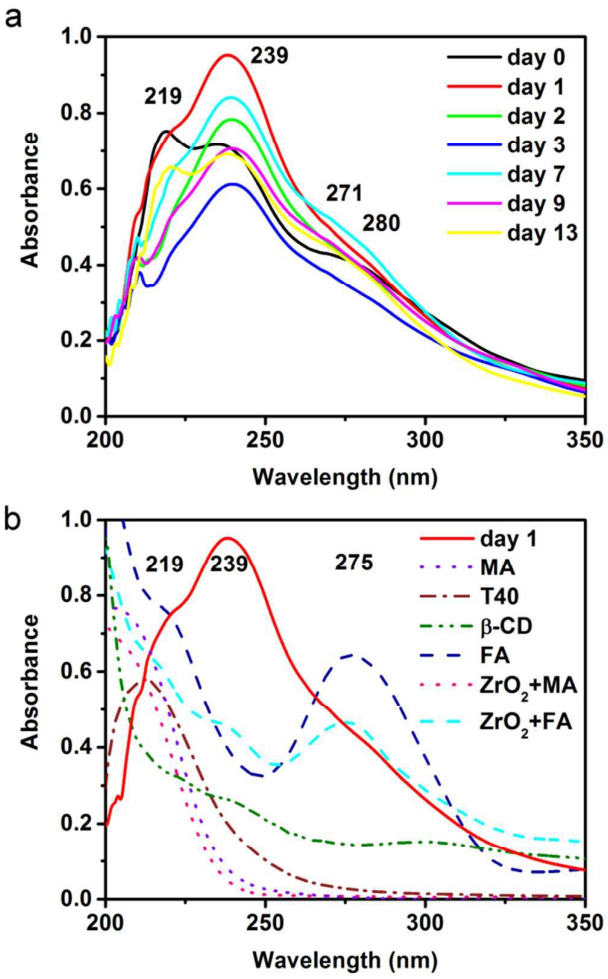

Figure 6 UV-visible spectra of (a) permeates obtained from dissolution of CN particles in physiological salt solution and (b) day 1 dissolution sample compared to those of polymeric shell components and suspensions of crystalline ZrO_2 powder in the presence of dissolved malic acid (MA) or folic acid (FA).

As the maximal intensity of the absorbance band observed at 239 nm is on the first day of dissolution, we assume that an amount of folic acid adsorbs directly to the surface of zirconia through carboxylic functional groups. The quick dissolution of these complexes suggests that the primary amine of these folates does not react in the polymerization reaction.

We further analysed the FTIR spectra of CN particles at the end of the above 14-days-period dissolution in saline and also that of the sample stirred in total cell medium (Fig.S-7 in ESI). We not only observed the notable change in polymeric bands (quality and quantity) in both media, but also the partial dissolution of silica and zirconia. The dissolution of silica has been reported earlier in the literature[17,18]. On the other hand, the biodegradation of zirconia resulting probably from folate complex formation has not yet been mentioned in the literature. The FTIR absorption bands of the CN polyester shell mainly disappeared from the spectrum and there remained the bands of polyamide (1647 cm^{-1} and 1553 cm^{-1}). The dissolution of silica is more pronounced in NaCl solution then in total cell medium. This difference is probably due to pH discrepancy between the two media (5.7 for saline and 7.8 for total cell medium).

The results of dissolution tests suggest that silica@zirconia cores would not remain for long time in the living organism but would dissolve completely within a few months.

Cell viability, radiolabeling and *in vivo* biodistribution

MTT assay was used to establish the cytotoxicity of CN nanoparticles applying primary rat hepatocytes. Cells were treated for 24 h with the indicated concentration of CN, and then the particles were washed out. Cell viability was assessed following the 24 h exposure (24 h) and 24 h later (48 h), in order to study the longer term effect of CN. (In the second 24 h term the cells were incubated without CN). Two-sample t-test performed on resulting data showed a concentration dependent decrease of cell viability (Fig.7).

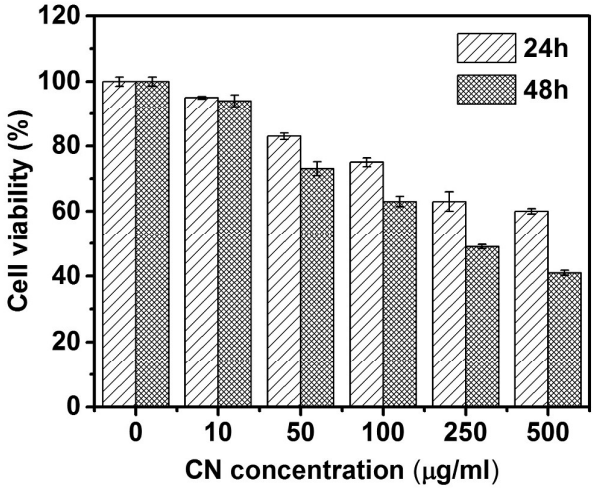

Figure 7 Cell viability assay carried out on hepatocyte cells for 24 h exposure and two incubation times and CN concentrations between 10-500 μg/ml.

The highest 0.5 mg/ml CN nanoparticle concentration reduced the viability to 63 ± 1 % and 43 ± 1 % of the control measured just after the exposure and at 48 h, respectively. Although NPs were washed out after 24 h exposure, the viability further decreased, which suggests that the NPs were retained in the hepatocytes, and/or initiated longer processes which lead to cell death.

The radiolabelling efficiency was determined 30 minutes, 3 hours and 20 hours postlabelling on the basis of TLC chromatograms (see chromatograms in Fig.S-8 in ESI). The radiolabelled products showed high degree (above 99%) and durable labelling efficiency during the entire *in vitro* follow-up study. We assume that the poly(ester-amide) backbone of the

View Article Online
DOI: 10.1039/C6TB01102K

polymeric shell with numerous pendant carboxyl groups acts as a polydentate chelator.

The *in vivo* biodistribution of the radiolabelled nanocarriers showed good correlation with products described earlier with similar particle size distribution[60]. Particles were quickly accumulated in the organs of the reticuloendothelial system (RES) (e.g. liver, spleen, bone marrow), and a smaller proportion of the radioactivity immediately started to wash-out through the urinary tract (kidneys, urinary bladder, urine). Clinical side effects in experimental animals were not recorded during the examinations. Out of the total injected activity, an average 48.4 % was accumulated in the liver (nearly 50 µg) and 9.0 % in the tumour (9 µg) in the first 30 minutes (Fig.8).

Figure 8 Photograph and overlaid SPECT/CT image of a He/De tumour transplanted Fischer rat 3 hours after 99mTc-labelled nanocarrier injection.

Organ activities demonstrated the slow elimination of nanocarrier. 8 hours post-injection almost 70% of the total injected activity was traceable by whole body ROI analysis. However, a retained blood-background could be observed which could be related to a relative long circulation time. Besides, a negligible uptake was detected in the thyroids, salivary gland, stomach mucosa and lungs, indicating that *in vivo* radiolabelling efficiency and particle diameters of the labelled nanocarriers were practically constant after i.v. application: particle aggregation did not occur. The obtained values of the organ activity uptakes are presented in Fig.S-9 in ESI. These findings confirm the suitability of CN sample for SPECT/CT application. CN particles were further applied for the diagnosis of folate receptor overexpressing tumours in spontaneously diseased veterinary patients (dog and cats). They have shown fair accumulation in oral carcinomas[60].

Conclusions

In this paper a novel, complex structure nanocarrier has been proposed with the prospect of theranostic application. The significance of this new nanocarrier lies in its versatility: the easy size tuning by means of the diameter of the silica core, and the one-step synthesis of the multifunctional polymeric shell surface-catalyzed by ZrO_2 coating, which allows the incorporation of any stable compounds bearing –OH, -COOH or $-NH_3$ functionality. The chelating property of the poly(ester-amide) backbone of the shell has allowed the efficient and stable radiolabelling with ^{99m}Tc, but we wish to demonstrate a more general chelating property in the future by conducting labelling experiments with other isotopes of shorter half-life. The present study did not give evidence of the presence of folic acid at the surface of complex nanocarriers. We, therefore, will proceed to the elucidation of this issue and carry out *in vitro* and *in vivo* biological experiments to observe folic acid targeting in a future study. We also aim to carry on characterization of hepatotoxic potential of NPs *in vitro*, and then to confirm the *in vitro* results *in vivo*.

CN particles and analogues with porous structure will further be applied for the encapsulation and release of small hydrophobic drugs. Such molecules are prone to form inclusion complexes with inbuilt β-cyclodextrin, hence, chemotherapy could be realized by the same pharmaceutical carrier as diagnosis and radiotherapy.

Acknowledgements

The authors gratefully acknowledge Teréz Kiss, Péter Németh and László Szabó for preliminary TEM experiments, as well as Kristóf Molnár for proofreading. This study was supported by Jedlik projects OM-00162/2007, 2007ALAP1-00070/2008 of the National Innovation Office (NIH, Hungary), the grant agreement CNK-81056 of the Hungarian Scientific Research Fund (OTKA, Hungary) and the Research Support of RCNS (2015.Bóta, No. 0609-15). The financial support did not take a share in publishing.

Notes and references

1 S. Mura and P. Couvreur, *Adv. Drug. Deliv. Rev.,* 2012, **64(13)**, 1394–1416.
2 X. Chen, S. S. Gambhir and J. Cheon, *Acc. Chem. Res.*, 2011, **44(10)**, 841–841.
3 E. Terreno, F. Uggeri and S. Aime, *J. Controlled Release*, 2012, **161(2)**, 328–337,
4 F. M. Kievit and M. Zhang, *Adv. Mater.*, 2011, **23(36)**, H217–H247.
5 R. Cheng, F. Meng, C. Deng, H. A. Klok and Z. Zhong, *Biomaterials*, 2013, **34(14)**, 3647–3657,
6 C. L. Modery-Pawlowski and A. Sen Gupta, *Biomaterials*, 2014, **35(9)**, 2568–2579.

View Article Online
DOI: 10.1039/C6TB01102K

7 T. Lammers, F. Kiessling, W. E. Hennink and G. Storm, *Mol. Pharm.*, **7(6)**, 1899–1912.
8 A. Polyak, I. Hajdu, M. Bodnar, Gy. Trencsenyi, Z. Postenyi, V. Haasz, G. Janoki, G. A. Janoki, L. Balogh and J. Borbely, *Int. J. Pharm.*, 2013, **449(1–2)**, 10–17.
9 D. Arcos and M. Vallet-Regí *Acta Mater.*, 2013, **61(3)**, 890–911.
10 R. Xing, A. A. Bhirde, S. Wang, X. Sun, G. Liu, Y. Hou and X. Chen, *Nano Res.*, 2013, **6(1)**, 1-9.
11 H. Yang, H. Mao, Z. Wan, A. Zhu, M. Guo, Y. Li, X. Li, J. Wan, X. Yang, X. Shuai and H. Chen, *Biomaterials*, 2013, **34**, 9124-9133.
12 I. J. Majoros and J. R. Baker, *Dendrimer-based nanomedicine*, Pan Stanford Publishing, Hackensack, NJ; 2008.
13 Y. Namiki, T. Fuchigami, N. Tada, R. Kawamura, S. Matsunuma, Y Kitamoto and M. Nakagawa, *Acc. Chem. Res.*, 2011, **44(10)**, 1080–1093.
14 M. Comes Franchini, G. Baldi, D. Bonacchi, D. Gentili, G. Giudetti, A. Lascialfari, M. Corti, P. Marmorato, J. Ponti, E. Micotti, U. Guerrini, L. Sironi, P. Gelosa, C. Ravagli and A. Ricci, *Small*, 2010, **6(3)**, 366-370.
15 L. Pradhan, R. Srivastava, D. Bahadur *Acta Biomater.*, 2014, **10**, 2976-2987.
16 X. He, X. Lin, K. Wang, L. Chen, P. Wu and Y. Yuan, in *Encyclopedia of Nanoscience and Nanotechnology*, ed. H. S. Nalwa, American Scientific Publishers, Valencia, CA; 2014, 235–253.
17 W. Zhai, C. He, L. Wu, Y. Zhou, H. Chen, J. Chang and H. Zhang, *J. Biomed. Mater. Res. B Appl. Biomater.*, 2012, **100(5)**, 1397–1403.
18 D. Shen, J. Yang, X. Li, L. Zhou, R. Zhang, W. Li, L. Chen, R. Wang, F. Zhang and D. Zhao, *Nano Lett.*, 2014, **14(2)** 923–932.
19 L. Wang, W. Zhao and W. Tan, *Nano Res.*, 2008, **1**, 99-115.
20 M. Pálmai, L. Naszályi Nagy, J. Mihály, Z. Varga, G. Tárkányi, R. Mizsei, I. Cs. Szigyártó, T. Kiss, T. Kremmer and A. Bóta, *J. Colloid Interface Sci.*, 2013, **390(1)**, 34–40.
21 W. Stöber, A. Fink and E. Bohn, *J Colloid Interface Sci.*, 1968, **26**, 62–69.
22 K. D. Hartlen, A. P. T. Athanasopoulos and V. Kitaev, *Langmuir*, 2008, **24(5)**, 1714–1720.
23 M. Hisbergues, S. Vendeville and P. Vendeville, *J. Biomed. Mater. Res. B Appl. Biomater.*, 2009, **88(2)**, 519–29.
24 R. J. Kohal, M. Bächle, W. Att, S. Chaar, B. Altmann, A. Renz, F. Butz, *Dent. Mater.*, 2013, **29(7)**, 763–776.
25 M. Srinivas and G. Buvaneswari, *Trends Biomaters. Artif. Organs*, 2006, **20(1)**, 24–30.
26 M. Catauro, M. Raucci and G. Ausanio, *J. Mater. Sci. Mater. Med.*, 2008, **19(2)**, 531–540.
27 C. Zhang, C. Li, J. Yang, Z. Cheng, Z. Hou, Y. Fan and J. Lin, *Langmuir*, 2009, **25(12)**, 7078–7083.
28 J. Widoniak, S. Eiden-Assmann and G. Maret, *Eur. J. Inorg. Chem.*, 2005, **15**, 3149–3155.
29 J. Kim, S. Chang, S. Kim, K. Kim, J. Kim and W. Kim, *Ceram. Int.*, 2009, **35**, 1243–1247.
30 S. Tang, X. Huang, X. Chen and N. Zheng, *Adv. Funct. Mater.*, 2010, **20(15)**, 2442–2447.
31 T. Kajiyama, H. Kobayashi, T. Taguchi, K. Kataoka and J. Tanaka, *Biomacromolecules*, 2004, **5**, 169–174.
32 T. R. Thatiparti, A. J. Shoffstall and H. A. von Recum, *Biomaterials*, 2010, **31(8)**, 2335–2347.
33 T. M. Allen and P. R. Cullis, *Adv. Drug Deliv. Rev.*, 2013, **65(1)**, 36–48.
34 S. M. Moghimi, A. C. Hunter and J. C. Murray, *FASEB J.*, 2005, **19(3)**, 311–330.
35 J. Sudimack and R. J. Lee, *Adv. Drug Deliv. Rev.*, 2000, **41(2)**, 147–162.
36 J. Telegdi, L. Trif, J. Mihály, E. Nagy and L. Nyikos, *J. Therm. Anal. Calorim.*, 2015, **121(2)**, 663-673.
37 C. Wagner, W. Riggs, L. Davis, J. Moulder and G. Muilenberg, *Handbook of X-Ray Photoelectron Spectroscopy*, Perkin-Elmer, Eden Prairie, MN; 1970.
38 J. Moulder, W Stickle, P. Sobol and K. Bomben, *Handbook of X-Ray Photoelectron Spectroscopy*, Perkin-Elmer, Eden Prairie, MN; 1992.
39 NIST Database (2015) http://srdata.nist.gov/xps/ (accessed August 2015)
40 P. Workman, E. O. Aboagy, F. Balkwill, A. Balmain, G. Bruder, D. J. Chaplin, J. A. Double, J. Everitt, D. A. H. Farningham, M. J. Glennie et al., *Br. J. Cancer*, 2010, **102(11)**, 1555–1577.
41 K. Greish, *Methods Mol. Biol.* (Clifton, NJ), 2010, **624**, 25–37.
42 R. K. Iler, *The chemistry of silica: solubility, polymerization, colloid and surface properties, and biochemistry*, Wiley, New York; 1979.
43 L. Naszályi, F. Bosc, A. El Mansouri, A. van der Lee, D. Cot, Z. Hórvölgyi and A. Ayral, *Sep. Purif. Technol.*, 2008, **59(3)**, 304–309.
44 C. Renger, P. Kushel, A. Kristoffersson, B. Clauss, W. Oppermann and W. Sigmund, *J. Ceram. Process. Res.*, 2006, **7(2)**, 106–112.
45 J. H. Choy and Y. S. Han, J. Mater. Chem., 1997, **7(9)**, 1815–1820.
46 B. Hua, G. Qian, M. Wang and K. Hirao, *J. Sol-Gel Sci. Technol.*, 2005, **33(2)**, 169–173.
47 J. Mihály, J. Kristóf, J. Mink, L. Nanni, D. Patracchini and A. D. Battisti, in *Progress in Fourier Transform Spectroscopy*, eds. J. Mink, G. Keresztury, R. Kellner, Springer, Vienna; 1997, 617–619.
48 R. M. C. Dawson ed., *Data for biochemical research*, Clarendon Press, Oxford; 1959.
49 G. Wohlfahrt, *Proteins Struct. Funct. Bioinforma.*, 2005, **58(2)**, 396–406.
50 L. Naszályi Nagy, J. Mihály, A. Polyak, B. Debreczeni, B. Császár, I. Cs. Szigyártó, A. Wacha, Zs. Czégény, E. Jakab, Sz. Klébert, E. Drotár, G. Dabasi, L. Balogh, A. Bóta and É. Kiss, *J. Mater. Chem. B*, 2015, **3**, 7529-7537.
51 A. Vora, A. Riga, D. Dollimore and K. S. Alexander, *Thermochim. Acta*, 2002, **392–393**, 209–220.
52 S. Kohata, K. Jyodoi and A. Ohyoshi, *Thermochim. Acta*, 1993, **217**, 187–198.
53 S. Han, C. Kim and D. Kwon, *Polym. Degrad. Stab.*, 1995, **47**, 203–208.
54 J. Portilla-Arias, M. García-Alvarez, A. Martínez de Ilarduya, E. Holler and S. Munoz-Guerra, *Biomacromolecules*, 2006, **7**, 3283–3290.
55 K. Takahashi, M. Shibagaki and H. Matsushita, *Bull. Chem. Soc. Jpn.*, 1989, **62**, 2353–2361.
56 G. Gyulai, C. B. Pénzes, M. Mohai, T. Lohner, P. Petrik, S. Kurunczi and É. Kiss, *J. Colloid Interface Sci.*, 2011, **362(2)**, 600-606.
57 M. G. A. El-Wahed, M. S. Refat and S. M. El-Megharbel, *Spectrochim. Acta A Mol. Biomol. Spectrosc.*, 2008, **70(4)**, 916–922.
58 L. Zhou, J. Xu, X. Li and F. Wang, *Mater. Chem. Phys.*, 2006, **97(1)**, 137–142.
59 A. Thomas, M. R. Feliz and A. L. Capparelli, *Transit. Met. Chem.*, 1996, **21(4)**, 317–321.
60 A. Polyak, L. Naszályi Nagy, A. Bóta, G. Dabasi, R. P. Jóba, G. Trencsényi, Z. Pösténvi, V. Haász, G. Jánoki and L. Balogh presented at *European Journal of Nuclear Medicine and Molecular Imaging*, Gothenburg, Sweden, Oct. 2014. doi: 10.1007/s00259-014-2901-9

View Article Online
DOI: 10.1039/C6TB01102K

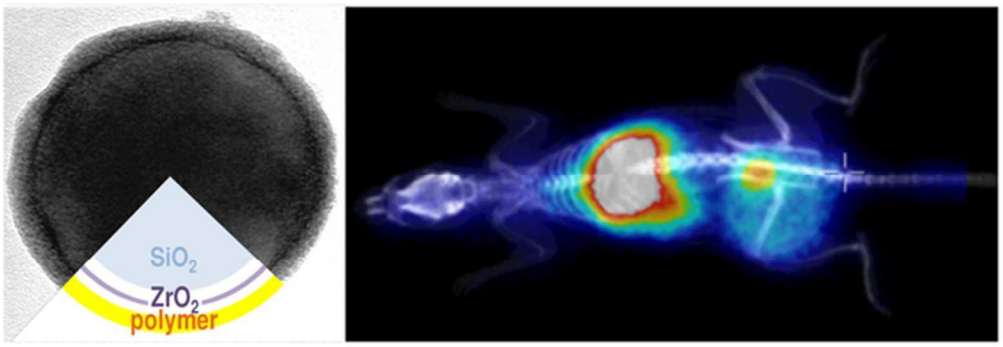

54x18mm (300 x 300 DPI)